Soft Matter

PAPER

View Article Online
View Journal | View Issue

A self-propelled thermophoretic microgear†

Cite this: *Soft Matter*, 2014, **10**, 1006

Mingcheng Yang*[ab] and Marisol Ripoll[a]

Received 13th September 2013
Accepted 2nd December 2013

DOI: 10.1039/c3sm52417e

www.rsc.org/softmatter

An asymmetric microgear will spontaneously and unidirectionally rotate if it is heated in a cool surrounding solvent. The resulting temperature gradient along the edges of the gear teeth translates in a directed thermophoretic force, which will exert a net torque on the gear. By means of computer simulations, the validity of this scenario is proved. The rotational direction and speed are dependent on gear–solvent interactions, and can be analytically related to system parameters like the thermal diffusion factor, the solvent viscosity, or the temperature difference. This microgear provides a simple way to extract net work from non-isothermal solutions, and can become a valuable tool in microfluids.

I. Introduction

Molecular motors usually refer to biological systems that operate in an environment where thermal fluctuations are significant, and that have an internal mechanism to convert energy into directed motion or mechanical work. These motors are ubiquitous in nature and play a crucial role in the transport within biological organisms. Examples are motor proteins moving along filaments[1] or bacteria swimming in low Reynolds number environments.[2] Such biological active matter has also been used to design nanomachines, as is the case of microgears pushed by a bacterial bath.[3,4] Inspired by nature, purely synthetic micromotors display self-propelled motion without biological components. These motors are receiving a rapidly increasing attention as a very promising avenue to realize purposeful functions on the micro and nanoscales. Various non-equilibrium strategies, with a breakdown of time reversal and spatial symmetries,[5] have been employed to build different synthetic micromotors.[6–13]

Recent experiments and simulations have shown that phoresis is a particularly appealing strategy to induce self-propelled motion.[14–20] Phoresis refers to the directed drift motion that suspended particles experience in inhomogeneous conditions. Important examples of such inhomogeneities are gradients of temperature (thermophoresis), concentration (diffusiophoresis), and electric potential (electrophoresis). In cases where the gradients are locally produced by the particles themselves, self-propulsion can occur. This is the case of a thermophoretic swimmer realized by laser heating a colloidal sphere half metal-coated.[18] Due to their simplicity and controllability, a benchmark investigation of the properties of active colloids has been experimentally performed with phoretic swimmers.[21,22] Phoretic micromotors have been designed until now by considering heterogeneous surface properties, as is the case of Janus particles and heterodimers to make swimmers, of twin and tethered Janus particles to build a rotor,[18] or of partially coated gears.[14] To find alternative designs of phoretic motors in general, and with homogeneous surfaces in particular, is challenging from a fundamental viewpoint, and has a great technological interest.

In this paper, we show that an asymmetric microgear with homogeneous surface properties rotates when heated in a cool surrounding solvent. The speed and direction of the microgear rotation are determined by its geometry, the interactions with the solvent, and the applied temperature differences. This can be experimentally realized by heating an asymmetric microgear with larger thermal conductivity than the solvent. Our results provide a novel route to design phoretic micromotors with homogeneous surfaces, which can be fueled by local heating.

II. Mesoscopic model

A hybrid simulation scheme in two dimensions is employed to model both the microgear and the surrounding solvent, whose typical time and length scales are separated by orders of magnitude. The nature of the problem imposes the necessity of reproducing stable temperature gradients, the effect of hydrodynamic interactions, and the conservation of angular momentum.[23] A particle-based mesoscopic simulation technique known as multiparticle collision dynamics (MPC)[24–28] is employed for the solvent, while the microgear and its interactions with the solvent are simulated by standard molecular dynamics (MD). The MPC dynamics consists of alternating streaming and collision steps. In the streaming step, the solvent particles of mass m move ballistically for a time h. In the collision step, particles are sorted into a square lattice with lattice

[a]*Theoretical Soft-Matter and Biophysics, Institute of Complex Systems, Forschungszentrum Jülich, 52425 Jülich, Germany. E-mail: mcyang@iphy.ac.cn; m.ripoll@fz-juelich.de*

[b]*Beijing National Laboratory for Condensed Matter Physics and Key Laboratory of Soft Matter Physics, Institute of Physics, Chinese Academy of Sciences, Beijing 100190, China*

† Electronic supplementary information (ESI) available. See DOI: 10.1039/c3sm52417e

size a, and interchange momentum relative to the center-of-mass velocity of each collision cell. In our simulations the stochastic rotation collision rule with variable collision angle α introduced by Ryder and Yeomans[29,30] is employed. This collision rule locally conserves mass, linear momentum, energy and angular momentum. It can therefore be proved that the algorithm properly captures hydrodynamic interactions, thermal fluctuations, and the sustainability of temperature inhomogeneities. Simulation units are reduced by setting $a = 1$, $m = 1$, and $k_B\tilde{T} = 1$ with k_B the Boltzmann constant and $\tilde{T}$ a reference temperature. We employ standard MPC parameters $h = 0.1$ and the mean number of solvent particles per cell $\rho = 10$. From the kinetic theory of the MPC with a fixed rotation angle $\alpha = 90°$,[31] we can approximately calculate the Schmidt number as $Sc = 12$, which corresponds to a liquid-like behavior. In our simulations, the kinematic viscosity is obtained to be $\nu = 0.46$, which is 40% smaller than the previous estimation.

The considered microgear is a solid structure where the surface is a sequence of sawteeth in a closed circular shape (Fig. 1). In our simulations, a gear with 8 teeth is used, with an internal radius $R_1 = 19a$ and an external radius $R_2 = 25a$. The short edge of each sawtooth is in the radial direction such that the tooth has angles $\theta_1 = 40°$ and $\theta_2 = 90°$. The microgear is surrounded by MPC solvent which is confined inside a circular wall with radius $R_w = 45a$. To obtain the solid gear structure two components are considered. One is a rigid gear with the sawteeth profile, with a momentum of inertia $I = 10^6 ma^2$. The rigid gear is free to rotate around its center fixed at the center of the simulation setup. Then a single-layer of monomer beads is mounted along the edges of the rigid gear, where the separation between neighboring beads is a. Each bead is attached to the rigid gear by a harmonic spring of constant $k = 600k_B\tilde{T}/a^2$. There are no further interactions between different beads. The external wall is similarly constructed by fixing beads with springs along an external circle. The coupling of the microgear and the solvent takes place through the MD bead–solvent particle interactions. The employed interaction is a Lennard-Jones (LJ) type potential[32,33] $U_k(r) = 4\varepsilon\left[\left(\frac{\sigma}{r}\right)^{2n} - \left(\frac{\sigma}{r}\right)^{n}\right] + c$ for $r \le r_c$. Here r is the distance between the bead center and the solvent particle, ε refers to the potential intensity, σ to the bead radius, and n to a positive integer describing the potential stiffness. The attractive or repulsive LJ potentials are obtained respectively by taking $c = 0$ or $c = \varepsilon$ with the corresponding cutoff r_c. The bead radius is taken as $\sigma = 1.25a$, and $\varepsilon = k_B\tilde{T}$. For efficiently exchanging energy with the surrounding solvent, the considered bead mass is $M = m$. A hard repulsive potential ($n = 24$, $c = \varepsilon$) is chosen for the external wall–solvent interactions, while both repulsive and attractive potentials are considered for the microgear–solvent interactions. Note that given the large overlap between neighboring beads (the separation between beads is 0.4 times their diameter) the solvent particles (not shown in Fig. 1) remain confined between the microgear and the circular wall. The equations of motion are integrated with a velocity-Verlet algorithm and a time step $\Delta t = h/50$.

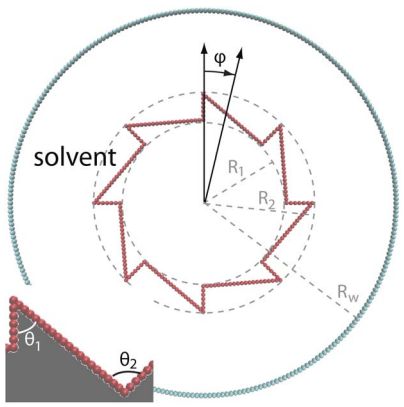

Fig. 1 Simulation setup of the eight-teeth microgear within a circular bead wall. Parameters are described in the main text.

The simulated microgear temperature T_g is uniformly imposed by independently thermostatting every bead in the gear edges every ten MD steps with a Maxwellian velocity distribution of temperature T_g, which is similar to the Andersen thermostat.[34] The thermosttating operation violates the conservation of the microgear angular momentum, which is then restored by adding or subtracting the corresponding small overall angular momentum. This compensation does not affect the microgear rotation, since the angular momentum variation in the thermostat operation slightly fluctuates around zero. Moreover, energy is drained from the system by thermostatting the wall beads with temperature T_w. By imposing the gear temperature increment $\Delta T = T_g - T_w$, a steady-state temperature distribution is quickly established (Fig. 2a). The environment of the solvent particles close to the summit and the cleft of each gear tooth is quite different (different size of the heating areas), such that the solvent temperature is different in both positions and varies along the edges. Moreover, a temperature jump is found at the solid–solvent interfaces, which is a consequence of the interfacial thermal resistance,[28,35,36] and has also been observed in recent simulation studies of heated nanobeads.[37–39] This temperature discontinuity could enhance the geometry-induced temperature gradient along the edges. We refer to ∇T_l and ∇T_s as the temperature gradients along the long and the short edges of each gear tooth (Fig. 2b). To the leading order, the gradients are expected to be proportional to the gear temperature increment, *e.g.* $|\nabla T_l| = \lambda_1 |\Delta T|$, with λ_1 a positive coefficient determined by the solid–solvent coupling and the gear geometry. In the example shown in Fig. 2c, $\lambda_1 \simeq (120a)^{-1}$. In the radial direction, the temperature varies logarithmically, as shown in Fig. 2d, which is a consequence of the conservation of energy.

The simulations performed here enforce the microgear constant temperature. Experimentally this corresponds to a microgear fabricated with a material of thermal conductivity much higher than that of the solvent, as it would be the case of a metal or a metal-coated microgear in water solution. However, the heat transport within the microgear is disregarded in our simulations given that the temperature is imposed by the use of a local thermostat. This is not relevant for our purpose, since the way in which the microgear constant temperature is imposed does not affect the solvent temperature distribution, nor the

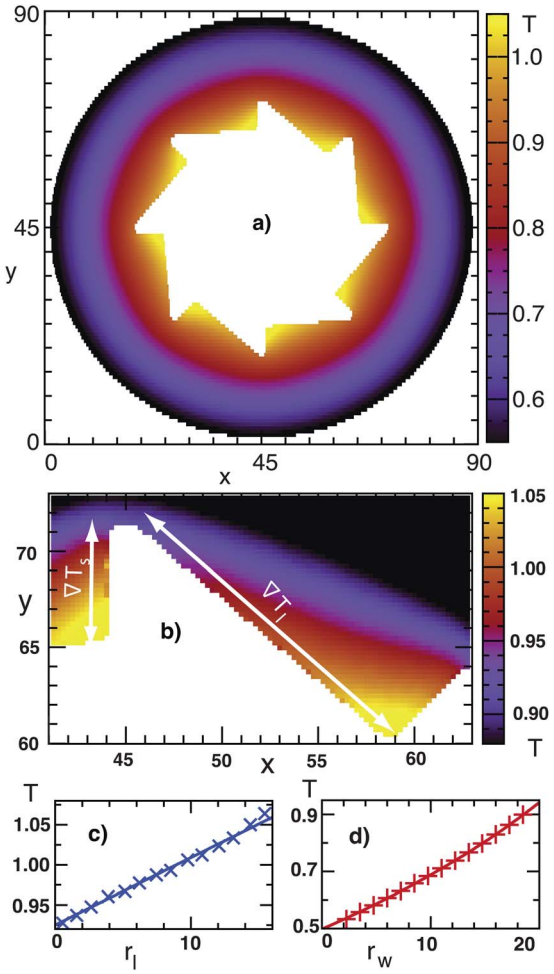

Fig. 2 (a) Steady state distribution of the solvent temperature with gear and wall temperatures fixed as $T_g = 1.5\bar{T}$ and $T_w = 0.5\bar{T}$, and gear-solvent soft repulsive interactions ($n = 3$, $c = \varepsilon$). (b) Zoom-in in the neighborhood of one gear tooth, indicating the temperature gradients ∇T_l and ∇T_s in the long and short edges. (c) Temperature along one of the long tooth edges, where r_l is the distance from one summit to the corresponding cleft. (d) Temperature as a function of r_w, the distance from the external wall to one of the tooth summits. Symbols in (c and d) correspond to simulation values and lines to data fits, in (c) the fit is linear and in (d) logarithmic.

solvent–gear interactions, and hence nor the gear motion. Alternatively, thermophoretic microgears can be constructed with materials of low or moderate thermal conductivity, and simulated with bead–bead interactions. Such microgears will not display a homogeneous temperature distribution, but a central temperature higher than that at the gear edges. The temperature at each summit will be lower than the temperature at the clefts. As a result, the temperature gradient of the solvent along the gear edge is still present, which is the crucial point for the motion of the hot microgear. Depending on the material properties, this temperature gradient can in principle be larger or smaller than in the case of the gear with constant temperature, which corresponds to a different value of λ_1 and therefore to a different gear rotation speed.

III. Results and discussion

A qualitative discussion of the microgear motion is first presented, followed by the simulation results, and a quantitative discussion. In the presence of a temperature gradient, a particle in solution experiences a thermophoretic drift force in the direction of the gradient.[40–42] This force is generated by the inhomogeneous interactions of the surrounding solvent with the particle.[43] When a solvent with a temperature gradient is in contact with a planar wall, only the tangential temperature gradient induces a thermophoretic force, which is then parallel to the wall. Thus, for our microgear ∇T_l and ∇T_s will respectively result in the thermophoretic forces on the long edges $f_{T,l}$ and the short edges $f_{T,s}$, parallel to the edges. Depending on the gear–solvent interactions,[32] the thermophoretic forces can be along (thermophilic) or against (thermophobic) the temperature gradient. Due to the gear geometry, the thermophoretic forces exert a non-vanishing torque $\mathscr{T} = \Sigma(R_l \times f_{T,l} + R_s \times f_{T,s})$ on the gear which results in its unidirectional rotation. Here, R_l and R_s respectively refer to the coordinates of the center of force on the long and short edges, and the summation accounts for multiple teeth. Besides the thermophoretic forces, the solvent exerts the standard pressure forces normal to the gear edges. The pressure forces on the short and long edges of the gear teeth produce torques in opposite directions that cancel each other. Note that in our simulations, given the very large overlap between neighboring beads, the edges of the microgear can be regarded as flat walls. Otherwise, for rough walls a normal temperature gradient will generate a thermophoretic force perpendicular to the wall. However, similar to the pressure forces, these normal forces would not result in any contribution to the net gear torque. Furthermore, in most of our simulations, the short tooth edge (hence R_s) and long tooth edge are, respectively, parallel and perpendicular to the radial direction. This means that only the forces applied in the long edges contribute to the total torque, and $|\mathscr{T}| \simeq 8R_1\,|f_{T,l}|$. A hot gear ($\Delta T > 0$) built of a thermophilic material will then rotate with the long teeth edges forward, which in the geometry of Fig. 1 is clockwise. Rotation in the opposite direction is then expected in the case of a cold microgear ($\Delta T < 0$), or when the material is thermophobic (see Fig. 3 and ref. 44). For a gear in equilibrium ($\Delta T = 0$) only pressure forces will be present, such that no net rotation is predicted.

The microgear rotation in the simulations is characterized by measuring rotation angle φ as illustrated in Fig. 1, where a positive φ corresponds to a clockwise motion. Simulation results of a thermophilic gear show in Fig. 3a an example of forward rotation for a hot gear ($\Delta T > 0$), backward rotation for a cold gear ($\Delta T < 0$), and no rotation in the case of a non-heated gear ($\Delta T = 0$). The averaged quantities consider a minimum of 8 independent runs. Fig. 3c shows an instantaneous gear trajectory where the unidirectional rotation can be observed to be simultaneously accompanied by thermal fluctuations (see also ref. 44). The thermophilic microgear is simulated by considering repulsive bead–solvent interactions ($n = 3$, $c = \varepsilon$).[32] Hot microgears with thermophobic behavior show in Fig. 3b the

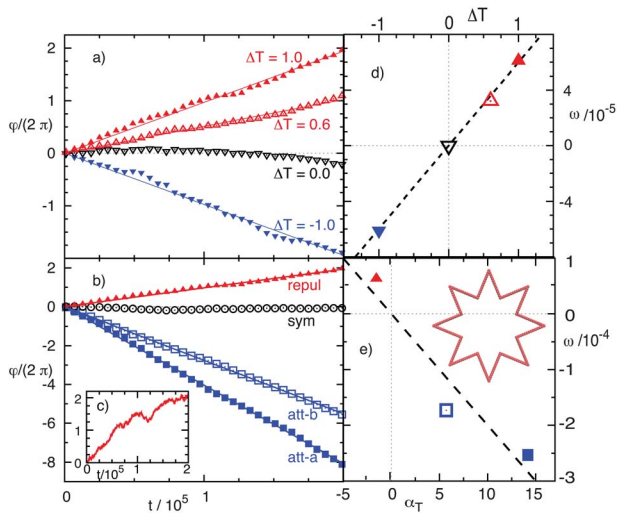

Fig. 3 (a–c) Rotational angle of the microgear as a function of time. Positive φ refers to rotation with the long edge forward. Symbols are simulation results and lines linear fits. (a) Averaged angle for repulsive gear repul ($n = 3$, $c = \varepsilon$) and various temperature increments. (b) Averaged angle for $\Delta T = 1.0$ and various interactions, att-a (full squares) refers to soft attractive gear ($n = 6$, $c = 0$), att-b (open squares) to hard attractive gear ($n = 10$, $c = 0$), and sym (circles) to a gear with symmetry geometry as depicted in the inset of (e). (c) Single run with $\Delta T = 1.0$ and repul. (d and e) Angular velocity as a function of ΔT, and the thermodiffusion factor α_T of a single surface bead in solution. Symbols correspond to the same parameters as in (a) and (b).

expected anticlockwise rotation. These thermophobic gears are simulated by attractive interactions ($c = 0$) of two different kinds of softness ($n = 6$, and $n = 10$). In all cases the self-induced rotation is due to the breakdown of the spatial symmetry produced by the asymmetric geometry of the heated microgear. We perform additional simulations for a microgear with symmetric teeth as displayed in the inset of Fig. 3e. The thermophoretic forces along both sides of each tooth are then symmetric with respect to the microgear radial direction, which results in a zero torque and vanishing net rotation (Fig. 3b).

In order to provide an expression for the rotation of the self-propelled microgear in terms of the material properties, the thermophoretic force on the long edge of the microgear needs to be explicitly calculated. For an isolated large suspended particle, f_T is well-accepted to be proportional to the temperature gradient ∇T with the so-called thermodiffusion factor α_T,[41–43]

$$f_T = -\alpha_T k_B \nabla T. \quad (1)$$

By definition $\alpha_T > 0$ corresponds to a thermophobic particle, and $\alpha_T < 0$ to a thermophilic particle. A bead embedded on the microgear interacts with the solvent only partially, such that its thermodiffusion factor $\alpha_{T,g}$ can be related to that of the isolated bead $\alpha_{T,g} = \lambda_2 \alpha_T$, with the dimensionless correction factor λ_2 ($0 < \lambda_2 < 1$). Independent simulations with a single bead are performed to quantify α_T for the different gear–solvent interactions used in Fig. 3e. This has been implemented by directly measuring the thermophoretic force on one isolated bead fixed in a solvent with an externally imposed temperature gradient.[32,45] The thermophoretic force on the long edge of the microgear then reads $f_{T,l} = -N_l \lambda_2 \alpha_T k_B \nabla T_l$ with $N_l = 20$ the number of beads on each long edge. Therefore, the effective thermodiffusion factor of the long edge is $\alpha_T^{ef} = N_l \lambda_2 \alpha_T$. This is a convenient concept when the constituent surface beads cannot be clearly identified, as in the case of most experimentally available systems. The torque exerted on the microgear is then

$$\mathcal{T} = -8 N_l \lambda_2 \alpha_T k_B R_1 \lambda_1 \Delta T \hat{z}, \quad (2)$$

with $\hat{z}$ the unit vector towards the plane. Here α_T is assumed to be temperature independent. The resulting angular velocity $\omega = \mu_r \mathcal{T}$, is proportional to the microgear rotational mobility μ_r. Regarding the microgear as a disk with hydrodynamic radius R_H, the mobility can be identified by $\mu_r = 1/(4\pi\eta R_H^2)$.[46] The angular velocity is then

$$\omega = -\frac{2\lambda_1 \lambda_2 N_l R_1}{\pi \eta R_H^2} \alpha_T k_B \Delta T \hat{z}. \quad (3)$$

The linear dependence of the rotation angle φ with time shown in Fig. 3a–c allows us to quantify the angular velocity ω of the gear in our simulations. The data in Fig. 3d and e are nicely consistent with linear dependence predicted by eqn (3) on ΔT and on α_T. A quantitative comparison of our simulation results with eqn (3) is non-trivial, since we do not really have a reliable measurement of parameters λ_2 and R_H in eqn (3). In the case of the repulsive gear with $\Delta T = 1.0$, we have measured λ_1, and the thermal diffusion factor $\alpha_T = -1.0$. The hydrodynamic radius can be considered to be the external gear radius $R_H \simeq R_2$, which together with the measured solvent viscosity, and ω, determines the factor $\lambda_2 \simeq 0.1$. This value is consistent with the fact that only 13% of the area of the microgear beads is in contact with the solvent. On the other hand it is important to note that, the essential mechanisms of this self-propelled microgear are the thermophoretic effect and the geometry-induced temperature gradient along the microgear edges, which are rather general and universal. Therefore, extensions of the model, like the consideration of the surface beads with internal degrees of freedom, and/or the gear with a temperature gradient inside (moderate heat conductivity), would cause only quantitative changes, leaving the essence of the device unchanged.

In order to emphasize the experimental feasibility and potential of the thermophoretic microgear, it is interesting to discuss a possible estimation of the orders of magnitude of the gear rotation speed ω. The rotational mobility of a 3 dimensional microgear is calculated as $\mu_r = 1/(4\pi\eta R_H^2 h_H)$,[46] with h_H the gear thickness. The gear hydrodynamic radius R_H, and the internal radius R_1 in eqn (2) will be of the same order of magnitude, such that the size dependence can be summarized as $\omega \sim \alpha_T^{ef}/(R_H h_H)$. The thermodiffusion factor α_T is well-known to be strongly dependent on particle size in general,[40] and in particular for diluted spherical colloids,[47,48] such that a significant dependence is also expected for flat surfaces. A polystyrene particle with 1 μm diameter in water has been characterized with $\alpha_T \sim 5000$.[49] Although there are no available experimental data to determine the relationship between α_T and α_T^{ef}, we can

for example consider a gear with the radius $R_H = 50$ μm, thickness $h_H = 1$ μm, and then in a similar spirit to our simulations we assume $\lambda_2 = 0.1$ and $N_l = 100$. This would correspond to a linear increase of α_T^{ef} with the length of the long edge, which would also be about R_H. Considering now the water viscosity $\eta \sim 0.001$ kg ms^{-1} and a temperature gradient $\nabla T = 0.1$ K μm^{-1}, it could be concluded that the microgear rotates ~1 round per second, which can be easily observed in experiments.

We want to bring the attention now to a related, but very different device that rotates in the presence of a self-induced temperature gradient, the well-known Crookes radiometer.[50–54] This radiometer is driven by thermal creep and works therefore for rarefied gases with typical sizes of millimeter. In contrast, the microgear presented here is driven by the thermophoretic effect in liquids, which is expected to work in microscales. The Crookes radiometer is built upon vanes with sides of different heat absorption, and therefore different temperatures. The rotation only happens on the cool side of the blade in the front. Meanwhile, the described thermophoretic microgear can rotate in both directions. Both the rotational direction and speed will change not only with the applied temperature increment but also with many other factors, related to the nature of the thermodiffusion factor. This factor is determined by composition of the gear and the fluid contained between the walls, and it will be affected by additional substances diluted in the fluid, or external conditions like pressure or average temperature. Moreover, the competition of thermophoresis with other effects like thermoelectricity[55,56] has interestingly shown the existence of materials whose properties vary from thermophobic to thermophilic. All these effects can provide a large versatility to this device. Correspondingly, the thermophoretic gear can become a very valuable tool to investigate the thermophoretic properties of a wide class of systems. Until now a requirement to determine the thermodiffusion factor, or equivalently the Soret coefficient, has been that the investigated system should be a solution. Therefore, materials systems that would for example precipitate in solution like gold in water could be investigated now by means of this new device.

IV. Conclusions

In conclusion, we have proved that an asymmetric microgear with homogeneous surface properties can spontaneously and unidirectionally rotate in solution, when the gear temperature is clearly distinguished from that of the environment. Our proof has been performed by means of computer simulations, but the effect is not restricted to the peculiarities of our model. Similar microrotor can also be realized experimentally, for example by heating a metallic microgear with a laser. When coupling the microrotor to an external device, net work could be extracted from nonisothermal solutions. As an example of other practical applications, our microrotor could be used as a stirring device, which could be locally controlled. Furthermore, when keeping the microgear fixed, the reaction of the thermophoretic force on the tooth edges can result in the motion of the surrounding fluid.[57] This can be employed to construct a thermophoretic pump, whose fluid motion is perpendicular to the applied temperature gradient.[58] Our findings provide an alternative strategy to design synthetic micromotors, which have become a promising tool in the field of microfluidics, and also in the investigation of thermal diffusion.

Acknowledgements

We would like to thank Andrea Costanzo and Simone Wiegand for valuable discussions. German patent application 102013007189.5 is pending for this work.

References

1 J. Howard, *Mechanics of Motor Proteins and the Cytoskeleton*, Sinauer, NewYork, 2000.
2 H. Berg, *E. coli in Motion*, Springer, NewYork, 2003.
3 L. Angelani, R. D. Leonardo and G. Ruocco, *Phys. Rev. Lett.*, 2009, **102**, 048104.
4 R. D. Leonardo, L. Angelani, D. DellArciprete, G. Ruocco, V. Iebba, S. Schippa, M. P. Conte, F. Mecarini, F. D. Angelis and E. D. Fabrizio, *Proc. Natl. Acad. Sci. U. S. A.*, 2010, **107**, 9541.
5 R. Feynman, *The Feynman lectures on physics*, Addison-Wesley, 1963.
6 R. D. Astumian and P. Hanggi, *Phys. Today*, 2002, **55**, 33.
7 P. Reimann, *Phys. Rep.*, 2002, **361**, 57.
8 W. F. Paxton, K. C. Kistler, C. C. Olmeda, A. Sen, S. K. S. Angelo, Y. Cao, T. E. Mallouk, P. E. Lammert and V. H. Crespi, *J. Am. Chem. Soc.*, 2004, **126**, 13424.
9 D. B. Weibel, P. Garstecki, D. Ryan, W. R. DiLuzio, M. Mayer, J. E. Seto and G. M. Whitesides, *Proc. Natl. Acad. Sci. U. S. A.*, 2005, **102**, 11963.
10 Y. Hiratsuka, M. Miyata, T. Tada and Q. P. Uyeda, *Proc. Natl. Acad. Sci. U. S. A.*, 2006, **103**, 13618.
11 A. Sokolov, M. M. Apodaca, B. A. Grzybowski and I. S. Aranson, *Proc. Natl. Acad. Sci. U. S. A.*, 2010, **107**, 969.
12 J. L. Anderson, *Annu. Rev. Fluid Mech.*, 1989, **21**, 61.
13 R. Golestanian, T. B. Liverpool and A. Ajdari, *Phys. Rev. Lett.*, 2005, **94**, 220801.
14 J. M. Catchmark, S. Subramanian and A. Sen, *Small*, 2005, **1**, 202.
15 J. R. Howse, R. A. L. Jones, A. J. Ryan, T. Gough, R. Vafabakhsh and R. Golestanian, *Phys. Rev. Lett.*, 2007, **99**, 048102.
16 G. Rückner and R. Kapral, *Phys. Rev. Lett.*, 2007, **98**, 150603.
17 L. F. Valadares, Y. G. Tao, N. S. Zacharia, V. Kitaev, F. Galembeck, R. Kapral and G. A. Ozin, *Small*, 2010, **6**, 565.
18 H. R. Jiang, N. Yoshinaga and M. Sano, *Phys. Rev. Lett.*, 2010, **105**, 268302.
19 M. Yang and M. Ripoll, *Phys. Rev. E: Stat., Nonlinear, Soft Matter Phys.*, 2011, **84**, 061401.
20 G. Volpe, I. Buttinoni, D. Vogt, H.-J. Kümmerer and C. Bechinger, *Soft Matter*, 2011, **7**, 8810.
21 J. Palacci, C. Cottin-Bizonne, C. Ybert and L. Bocquet, *Phys. Rev. Lett.*, 2010, **105**, 088304.

22 I. Theurkauff, C. Cottin-Bizonne, J. Palacci, C. Ybert and L. Bocquet, *Phys. Rev. Lett.*, 2012, **108**, 268303.
23 I. O. Götze, H. Noguchi and G. Gompper, *Phys. Rev. E: Stat., Nonlinear, Soft Matter Phys.*, 2007, **76**, 046705.
24 A. Malevanets and R. Kapral, *J. Chem. Phys.*, 1999, **110**, 8605.
25 M. Ripoll, K. Mussawisade, R. G. Winkler and G. Gompper, *Phys. Rev. E: Stat., Nonlinear, Soft Matter Phys.*, 2005, **72**, 016701.
26 J. T. Padding and A. A. Louis, *Phys. Rev. E: Stat., Nonlinear, Soft Matter Phys.*, 2006, **93**, 031402.
27 R. Kapral, *Adv. Chem. Phys.*, 2008, **140**, 89.
28 D. Lüsebrink and M. Ripoll, *J. Chem. Phys.*, 2012, **136**, 084106.
29 J. F. Ryder, Mesoscopic Simulations of Complex Fluids, Ph.D. thesis, University of Oxford, 2005.
30 G. Gompper, T. Ihle, D. M. Kroll and R. G. Winkler, *Adv. Polym. Sci.*, 2009, **221**, 1.
31 E. Tüzel, T. Ihle and D. M. Kroll, *Phys. Rev. E: Stat., Nonlinear, Soft Matter Phys.*, 2006, **74**, 056702.
32 D. Lüsebrink, M. Yang and M. Ripoll, *J. Phys.: Condens. Matter*, 2012, **24**, 284132.
33 G. A. Vliegenthart, J. F. M. Lodge and H. N. W. Lekkerkerker, *Phys. A*, 1999, **263**, 378.
34 H. C. Andersen, *J. Chem. Phys.*, 1980, **72**, 2384.
35 D. Rings, R. Schachoff, M. Selmke, F. Cichos and K. Kroy, *Phys. Rev. Lett.*, 2010, **105**, 090604.
36 O. M. Wilson, X. Hu, D. G. Cahill and P. V. Braun, *Phys. Rev. B: Condens. Matter Mater. Phys.*, 2002, **66**, 224301.
37 S. Merabia, S. Shenogin, L. Joly, P. Keblinski and J. L. Barrat, *Proc. Natl. Acad. Sci. U. S. A.*, 2009, **106**, 15113.
38 L. Joly, S. Merabia and J. L. Barrat, *EPL*, 2011, **94**, 50007.
39 D. Chakraborty, M. V. Gnann, D. Rings, J. Glaser, F. Otto, F. Cichos and K. Kroy, *EPL*, 2011, **96**, 60009.
40 S. Wiegand, *J. Phys.: Condens. Matter*, 2004, **16**, R357.
41 R. Piazza and A. Parola, *J. Phys.: Condens. Matter*, 2008, **20**, 153102.
42 A. Würger, *Rep. Prog. Phys.*, 2010, **73**, 126601.
43 M. Yang and M. Ripoll, *J. Phys.: Condens. Matter*, 2012, **24**, 195101.
44 For movies illustrating the microgear rotation see ESI.†
45 G. Galliéro and S. Volz, *J. Chem. Phys.*, 2008, **128**, 064505.
46 P. G. Saffman and M. Delbrück, *Proc. Natl. Acad. Sci. U. S. A.*, 1975, **72**, 3111.
47 S. Duhr and D. Braun, *Phys. Rev. Lett.*, 2006, **96**, 168301.
48 M. Braibanti, D. Vigolo and R. Piazza, *Phys. Rev. Lett.*, 2008, **100**, 108303.
49 F. M. Weinert and D. Braun, *Phys. Rev. Lett.*, 2008, **101**, 168301.
50 J. C. Maxwell, *Proc. R. Soc. London*, 1878, **27**, 304.
51 R. Piazza, *J. Phys.: Condens. Matter*, 2004, **16**, S4195.
52 L. H. Han, S. Wu, J. C. Condit, N. J. Kemp, T. E. Milner, M. D. Feldman and S. Chen, *Appl. Phys. Lett.*, 2010, **96**, 213509.
53 A. A. Donkov, S. Tiwari, T. Liang, S. Hardt, A. Klar and W. Ye, *Phys. Rev. E: Stat., Nonlinear, Soft Matter Phys.*, 2011, **84**, 016304.
54 A. Würger, *Phys. Rev. Lett.*, 2011, **107**, 164502.
55 D. Vigolo, S. Buzzaccaro and R. Piazza, *Langmuir*, 2010, **26**, 7792.
56 A. Würger, *Phys. Rev. Lett.*, 2008, **101**, 108302.
57 M. Yang and M. Ripoll, *Soft Matter*, 2013, **9**, 4661.
58 M. Yang and M. Ripoll 2013, preprint.